Why Deep Learning Works: A Manifold Disentanglement Perspective

Pratik Prabhanjan Brahma, Dapeng Wu, *Fellow, IEEE*, and Yiyuan She

***Abstract*— Deep hierarchical representations of the data have been found out to provide better informative features for several machine learning applications. In addition, multilayer neural networks surprisingly tend to achieve better performance when they are subject to an unsupervised pretraining. The booming of deep learning motivates researchers to identify the factors that contribute to its success. One possible reason identified is the flattening of manifold-shaped data in higher layers of neural networks. However, it is not clear how to measure the flattening of such manifold-shaped data and what amount of flattening a deep neural network can achieve. For the first time, this paper provides quantitative evidence to validate the flattening hypothesis. To achieve this, we propose a few quantities for measuring manifold entanglement under certain assumptions and conduct experiments with both synthetic and real-world data. Our experimental results validate the proposition and lead to new insights on deep learning.**

***Index Terms*— Deep learning, disentanglement, manifold learning, unsupervised feature transformation.**

I. Introduction

THE ADVENT of artificial neural networks ignited a quantum shift from the linear machine learning methods. Neural networks, using multiple hidden layers, have very high capacity to model highly varying functions defining the nonlinear structure of input data. However, multilayer neural networks face a critical problem that the lower layers remain undertrained as their corresponding gradients get diminished while using backpropagation [1]. Very often, a neural network gets stuck in either a local minima or a saddle point [2], and the adaptive gradient descent fails to move on from there. Although several heuristic solutions have been suggested, the problems of poor local minima and overfitting in neural networks have been among the primary reasons that led to the subsequent decrease in popularity. Kernel methods [3], with a strong theoretical foundation, paved the way for the third generation machine learning algorithms and proved to be the state of the art in cases, such as speaker identification [4] and text categorization [5]. These methods project the data to a very high (even infinite) dimensional space without explicitly worrying about the mapping function and comfortably assume that the linear regression and classification methods can be used consequently. However, these methods depend on using a kernel function that is usually predefined and hence, in general, not data adaptive. The discussion in [6] shows that a large number of training examples is required in the case of local kernels, such as Gaussian, even if the Kolmogorov complexity of the target function may be low. Recent research works [7] have pointed out that the deep architectures, such as multilayer neural networks, showed better performance when the traditional backpropagation algorithm was preceded by an unsupervised pretraining. These designs can also be thought of as kernel methods with a data-dependent Gram matrix. This brought back the interest of the academic fraternity into multilayer neural networks again, and deep learning methods [4] have since excelled in being the top performer in many applications, such as object detection and recognition, handwriting recognition [8], speaker identification [9], and text mining [7].

Though a concrete mathematical reasoning of the success behind these techniques is yet unclear, several intuitive reasons have been articulated in [10] and [11]. One of the ideas is based on the manifold perspective where it is hypothesized that the deeper layers can help extract the underlying factors of variations that define the structure of the data geometrically. Through the learning process, the data manifolds are unfolded and flattened, so that the subsequent processing using the output features can be made easier. A feature space that can correctly represent the hidden factors underlying observed data is better to deal with for further learning [12]. For example, in prediction or interpolation, if we can flatten [13] or linearize the complicated manifolds along the factors that led to the generation of data, then the task can be performed easily using even linear regression techniques. Researchers, such as in [14], have attempted to measure invariance across layers in a deep network. However, these measures are not based on the structural connectivity of the data points and may not be suitable to quantify the extent to which disentanglement of manifolds is achieved under the deep learning paradigm. Novel degrees of entanglement, based on the manifold hypothesis, have been designed and tested in this paper to quantitatively show the unfolding of class specific manifolds in the data.

The remainder of this paper is organized as follows. Following the introduction, Section II deals with a brief introduction

Manuscript received November 7, 2014; revised January 26, 2015, June 28, 2015, and October 21, 2015; accepted October 22, 2015. Date of publication December 7, 2015; date of current version September 15, 2016. This work was supported in part by the National Science Foundation under Grant DMS-1352259 and in part by the National Natural Science Foundation of China under Grant 61529101. *(Corresponding author: Dapeng Wu.)*

P. P. Brahma and D. Wu are with the Department of Electrical and Computer Engineering, University of Florida, Gainesville, FL 32611 USA (e-mail: prprbr@ufl.edu; wu@ece.ufl.edu).

Y. She is with the Department of Statistics, Florida State University, Tallahassee, FL 32306 USA (e-mail: yshe@stat.fsu.edu).

Color versions of one or more of the figures in this paper are available online at http://ieeexplore.ieee.org.

Digital Object Identifier 10.1109/TNNLS.2015.2496947

to deep learning methods and, especially, the unsupervised pretraining techniques. Section III lays out the fundamental definitions of manifolds and explains the popular hypothesis of real-world data containing intrinsically low-dimensional manifolds embedded in high-dimensional space. In Section IV, we design metrics from a differential geometry perspective to quantify the entanglement of a nonlinear manifold with respect to a completely flat or linear subspace. These measures are then used in Section V on features obtained from different layers of deep neural networks when applied onto synthetic and real-world image data sets. Finally, the conclusion is drawn in Section VI.

II. Deep Learning Methods

Multilayer neural networks have large capacity to model a high degree of nonlinearity in the input data but face the problems of poor training of lower layers, getting stuck in unwanted local optima and overfitting. However, it was the unsupervised pretraining introduced in [7] that gave a new dimension to the deep learning research. It discusses an undirected graphical model, called Boltzmann machine, consisting of hidden (h_i) and visible (x_i) nodes. The joint probability of the clique is given as

$$P(x,h) = \frac{e^{-E(x,h)}}{Z} \tag{1}$$

where $E(x,h)$ is the energy function describing the interactions in the graphical model that behaves as a Markov random field. Z is the partition function which acts as a normalization to make $P(x,h)$ a probability measure. The energy function for a restricted Boltzmann machine (RBM), where there are no intrahidden or intravisible interactions, is given by a simple equation

$$E(x,h) = -b'x - c'h - h'\mathbf{W}x \tag{2}$$

where $\Theta = \{b, c, \mathbf{W}\}$ is the set of model parameters. Due to the bipartite restrictions put on an RBM, the hidden nodes are independent of each other when conditioned on the visible nodes and vice versa as shown in

$$P(h|x) = \prod_{i \in \text{Hid}} P(h_i|x). \tag{3}$$

The individual conditional probabilities turn out to be a simple sigmoid function when both the hidden and visible nodes are conditioned to be taking only binary values

$$P(h_i|x) = \text{sigm}\left(c_i + \sum_{j \in \text{Vis}} W_{ji}x_j\right). \tag{4}$$

In general, it is desired to create a generative model, so that the hidden nodes can learn to generate new model data in accordance to the actual probability density function of the input data. Thus, its log likelihood is set to be maximized in the objective function. Although it involves intractable parameters such as the partition function Z, a slightly biased sampling procedure called contrastive divergence [15] is used by constructing model visible and hidden features through consecutive Gibbs sampling. The overall gradient of the log likelihood, that is, to be used as the weight update, is given as

$$\Delta w_{ij} = \eta(\langle h_i x_j \rangle_{\text{original}} - \langle h_i x_j \rangle_{\text{reconstruction}}) \tag{5}$$

where $\langle , \rangle$ (inner product) calculates the number of times the ith hidden and jth visible nodes are simultaneously ON. Similarly, the biases b and c can also be trained iteratively using the gradient information. The above analysis can also be extended to both hidden and visible nodes being characterized by Gaussian random variables by changing the energy function to

$$E(x,h) = \sum_{\text{vis}} \frac{(x_i - a_i)^2}{2\sigma_i^2} + \sum_{\text{hid}} \frac{(h_j - b_j)^2}{2\sigma_j^2} - \sum_{i,j} W_{ij}\frac{x_i h_j}{\sigma_i \sigma_j}. \tag{6}$$

Such a graphical model can be trained using the continuous RBM learning algorithm given in [16].

The concept of depth in a deep belief network (DBN) comes from stacking RBMs on top of one another and greedily training them. The weights and the biases obtained after the unsupervised pretraining then act as a starting setup for a neural network that can be further trained using supervised backpropagation. It has been shown to serve as a better initialization as compared with traditionally performed random initialization. Out of the several intuitions that have come up on why such an unsupervised pretraining helps, we hereby state and experimentally validate one that is based on the disentanglement of manifolds present in the data.

Other than the DBN approach discussed above, there are other popular designs for multilayer neural architectures [4] too, such as stacked denoising autoencoders, deep Boltzmann machine, and convolutional neural networks. Apart from neural networks, the stacking blocks can also be replaced with random projections [17] or spectral embedding too. Most of the deep learning paradigms share an unsupervised pretraining method, and it is thus important to understand the impact of this stage on the overall model's behavior. As will be shown later, it is the amalgamation of generative and discriminative model design that leads to better performance in any machine learning task. Although only the DBN architecture is considered for all the experiments in this paper, the performance evaluation metrics developed here can also be used to test other types of deep learning designs like the ones mentioned above.

III. Manifold Concepts

Definition 1: A topological space [18] (a set of points along with neighborhood for each point) is a topological manifold M if and only if the following condition holds.

1) M is the Hausdorff (distinct points have disjoint neighborhood).
2) M is the second countable (there exists a countable basis to the topology of M).
3) M is also locally Euclidean, i.e., $\forall p \in M, \exists$ an open set $U \subset M$ containing p that has a homeomorphism $\varphi : U \to V$ (a mapping function with a continuous inverse) with an open set $V \subset \mathbb{R}^n$.

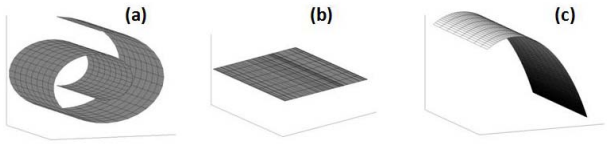

Fig. 1. Comparison of (a) an entangled nonlinear manifold, (b) a flat linear manifold, and (c) a slightly disentangled manifold.

As an example shown in the leftmost figure of Fig. 1, a swiss roll in $\mathbb{R}^3$ is actually a two-manifold. A pair (U, φ) is called a coordinate chart. An atlas for M is defined to be a collection of charts whose domains cover the entire M. An atlas A is called a smooth atlas if any two charts in A are smoothly compatible with each other.

Definition 2: A smooth manifold is a topological n-manifold with a smooth atlas A of M.

The sphere S^2 lying in $\mathbb{R}^3$ is a smooth two-manifold. The rest of this paper assumes that the data in each of the categories, such as all the images belonging to a single person, lie on a smooth-connected manifold.

Most real-world data are assumed to lie in a complicated nonlinear manifold fashion. The manifold hypothesis [19] suggests that the complex data manifolds are intrinsically low dimensional. It means that the manifold has a local homeomorphism with a Euclidean space of dimensionality lower than the original space. For instance, the pictures of a human face may have pixels of the order of millions depending on the resolution of the camera. However, the images can be characterized using a few factors of variation [20], such as lighting, orientation, shades, shape, and pose. According to the hypothesis, if the underlying factors of variation can be discovered appropriately, the projected data in its intrinsic form will exhibit flatter or linearized geometry and learning tasks like classification become easier, possibly using even a linear classifier. This has been the basis for several nonlinear dimensionality reduction techniques. A linear manifold is rather less complicated to deal with and is actually just a linear subspace that has possibly been shifted away from the origin $\mathbf{0}$.

Definition 3: A nonempty subset L of a vector space V is a linear subspace or a linear manifold if along with every pair, x and y, of vectors contained in L, every linear combination $\alpha x + \beta y$ is also contained in L. While a linear subspace has to contain the $\mathbf{0}$ vector in it, the linear manifold may or may not pass through the origin.

Points and lines in $\mathbb{R}^2$ and points, lines, and flat planes in $\mathbb{R}^3$ are the examples of linear manifolds. It is easier to learn from data lying on such linear hyperplanes as compared to nonlinear manifolds, be it for classification and regression, as conventional linear methods can be directly applied.

For nonlinear manifolds, various manifold learning algorithms [19], such as ISOMAP, local linear embedding, Laplacian eigenmaps, and others, have been developed. These methods have been shown to clearly outclass their linear counterparts, such as principal component analysis (PCA). A simple pictorial illustration is given in Fig. 1 where a swiss roll, intrinsically 2-D, cannot be reduced to its original $\mathbb{R}^2$ version by just applying PCA. However, when it is unfolded into linear varieties or even substantially disentangled versions, as shown in Fig. 1(b) and (c), the task of subspace learning is made easier. It is worth noting here that a 2-D PCA projection of Fig. 1(c) can also serve the purpose if, for instance, classification between two half portions of the swiss roll was the learning objective. Most of these manifold learning methods try to project an isometric embedding of the data onto a low-dimensional space but fail to produce an explicit feature transformation function that can be readily applied onto new test data. In addition, these methods are severely limited by the choice of neighborhood.

It was first proposed in [11] that the regularized autoencoders tend to disentangle the complex manifold structures in data by unfolding and volume expansion. They showed that the linear mixing between feature vectors in the higher layers can help generate more plausible training examples using the decoder. This is possible only when the projection of the manifold in the higher layers is linear as suggested in Definition 3. The data exhibit high probability concentration along the low-dimensional manifold, and it drastically reduces as one goes away from it. The intuition is that a hidden representation can capture the variations along the manifold in input space and ignore the variations orthogonal to the tangent spaces of the manifold. Since an RBM or any regularized autoencoder is designed on the connection between a set of hidden and visible variables, it is argued in [11] that the hidden variables can be the representative of the governing variations in the visible input space. However, it is worth investigating how much success is achieved by a deep architecture in the objective of linearizing the data manifolds. In a classification paradigm, each class present in the data can be modeled as a nonlinear manifold itself, and thus, the data are the composition of jumbled manifolds, just like each mode in a multimodal distribution. Disentanglement aims at extracting the inherent features that can then be used as input to a simple classifier. It is worth mentioning here that just unfolding alone may not necessarily mean better classification as the disentangled linear hypersurfaces may still be intersecting. However, as it is shown as a sanity check in [10], the deep network unfolds as well as separates the class structures. For the rest of this paper, the concept of disentanglement can be understood as flattening as well as separating the individual data manifolds for respective classes. As will be shown later in this paper, disentanglement is maintained and even pronounced after discriminative backpropagation, which helps in achieving good classification.

IV. Measures of Entanglement

In this section, we are interested in indicating how much the individual class manifolds have unfolded with respect to the original structures formed by the actual data points. In order to quantify this process, we make use of distances between the training examples. Distances can be Euclidean (l_2-norm of the distance vector) or can be geodesic in nature.

Definition 4: A geodesic distance [18] on a Riemannian manifold M between two points p and q on the manifold is

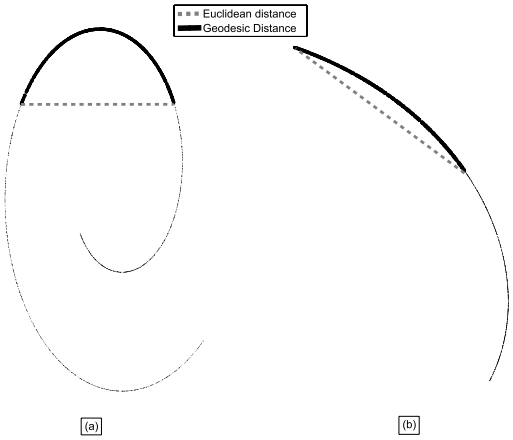

Fig. 2. Geodesic and Euclidean distances for (a) entangled and (b) slightly disentangled manifolds.

defined as the infimum of the lengths taken over all piecewise continuously differentiable curves $\gamma : [a, b] \rightarrow M$, where $\gamma(a) = p$ and $\gamma(b) = q$.

In other words, these distances are locally length-minimizing paths inscribed on the manifold. Although intractable without given the exact function defining the geometry, it can be approximated using the graph geodesic distance [21]. A nearest neighbor graph can be formed out of the given P-dimensional data samples $x_i \in \mathbb{R}^P$, and the shortest path between two points is a geodesic path approximately traversed along the manifold surface. Let the total number of data samples be N. The sum of the individual Euclidean distances serves as an estimate for the manifold distance as given by

$$G_M(i, j) = \sum_k |e_k| \tag{7}$$

where $|e_k|$ denotes the lengths of the k edges contained in the shortest path connecting x_i and x_j data nodes. The pairwise Euclidean distances are stored in an $N \times N$ matrix as

$$G_E(i, j) = \|\mathbf{x}_i - \mathbf{x}_j\|_2. \tag{8}$$

Let $\mathbf{r}_E$ and $\mathbf{r}_M$ be vectors formed by concatenation of the upper triangular entries of symmetric matrices G_E and G_M, respectively. Thus, both $\mathbf{r}_E$ and $\mathbf{r}_M \in \mathbb{R}^{N(N-1)/2}$. The Euclidean distance is also the geodesic distance between two points lying on a linear manifold. As shown in Fig. 2, the geodesic and Euclidean distances tend to be closer to each other as the manifold gets more and more unfolded. The first measure, based on similarity between geodesic and Euclidean distances, is the residual normalized cross correlation between $\mathbf{r}_E$ and $\mathbf{r}_M$. Let c_k be defined as

$$c_k = 1 - \frac{(r_M(k) - \mu_{r_M})(r_E(k) - \mu_{r_E})}{\sigma_{r_M}\sigma_{r_E}} \tag{9}$$

where μ_{r_M} and μ_{r_E} are the means, and σ_{r_M} and σ_{r_E} are the standard deviations of $\mathbf{r}_E$ and $\mathbf{r}_M$, respectively. The first measure can then be written as

$$\tilde{c} = \frac{2}{N(N-1)} \sum_k c_k = E[c]. \tag{10}$$

The second measure is again another average value of the difference between distinct ($i \neq j$) pairwise Euclidean and geodesic distances normalized by its corresponding Euclidean distance and is given by

$$\tilde{d} = \frac{2}{N(N-1)} \sum_{(i,j)} \frac{|G_M(i, j) - G_E(i, j)|}{|G_E(i, j)|} = E[d]. \tag{11}$$

Both the definitions of $\tilde{d}$ and $\tilde{c}$ involve an averaging using the mean operator. However, the simple mean cannot be a robust measure for highly noisy data, which may also contain outliers lying far away from the intrinsic manifold structure. To increase the robustness of the measures, we propose using the α-trimmed mean. This chops off the most extreme values, both low and high, of all the entries c_k and d_{ij} in (10) and (11) from being considered. The general form for the α-trimmed mean for any vector $Y \in \mathbb{R}^{n\times 1}$ is given as

$$E^{\alpha}[Y] = \frac{1}{n - 2\alpha n} \sum_{i=\alpha n+1}^{n-\alpha n} Y_{(i)} \tag{12}$$

where $Y_1 \leq Y_2 \leq Y_3 \cdots \leq Y_n$ are the entries of the vector Y sorted in an increasing order. Similarly, $\tilde{d}^{\alpha}$ and $\tilde{c}^{\alpha}$ are the robust α-trimmed versions of the measures introduced earlier in this section.

Together with robustness, the measures should also remain sensitive to the slightest of disentanglement. For this, a close neighborhood for each point is ignored as the measures remain indifferent for that region in both a flat manifold and a nonflat manifold. For each point x_i, we take $\mathscr{S}$ number of neighbors in which $G_M(i, j)$ and $G_E(i, j)$, for a certain point x_j in that $\mathscr{S}$-neighborhood of x_i, are going to be almost similar to each other and will thus have a high correlation too. In order to make the measures sensitive, distances for these nearby pairs should be ignored from the computation. The decision that two points x_j and x_i are not lying in the considered neighborhood range is denoted by $\mathscr{S}(i, j)$ being not equal to 0, and thus, the measures can now be modulated as

$$\tilde{d}^{\mathscr{S}} = E_{\mathscr{S}(i,j)\neq 0}[d] \tag{13}$$

and

$$\tilde{c}^{\mathscr{S}} = E_{\mathscr{S}(i,j)\neq 0}[c]. \tag{14}$$

Both sensitivity and robustness are considered while computing our measures $\tilde{d}^{\mathscr{S},\alpha}$ and $\tilde{c}^{\mathscr{S},\alpha}$, which are henceforth referred to as simply d and c, respectively. Through experiments on synthetic and real-world image data sets, it has been observed that the measures do not change much with the tuning of parameters α and $\mathscr{S}$. However, if these are taken to be very high, we end up losing a lot of information about the manifold structure of the data and its variation across the layers of a deep learning network. Similarly, closer to zero values of α and $\mathscr{S}$ may make the measures of entanglement susceptible to noise and outliers. Smaller values of d occur when the pairwise geodesic and Euclidean distances have values closer to each other, whereas smaller values of c would mean that the pairwise geodesic and Euclidean distances are more correlated with each other, i.e., two points farther away from each other with respect to the l_2 norm are also farther

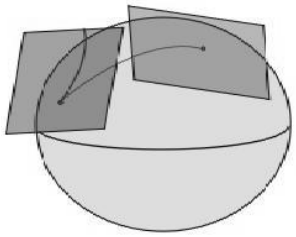

Fig. 3. Alignment of tangent spaces along a geodesic path.

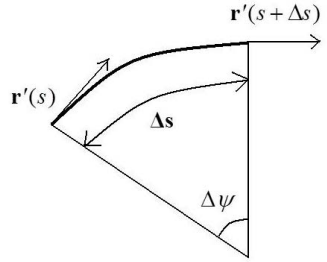

Fig. 4. Calculating curvature from changing tangent space along the surface of a manifold.

away in a geodesic sense. Reduction of both the measures will suggest that the manifold is more unfolded or flattened. For an ideal flat manifold, the values of both c and d should be equal to 0.

The advantages of choosing such forms for the measures are that these are now both translation and rotation invariant, since the distances between samples are not affected as long as the geometry is maintained. In addition, any isotropic scaling of the data matrix by a multiplicative scalar will cause the numerator and denominator in both (10) and (11) to change by the same order and hence canceling out the effect on the resultant values of c and d. Thus, any change in these measures has to be due to a geometrical modification of the structure of the data manifold.

As shown in Fig. 3, one can also use the alignment of the tangent space estimated at different locations on a geodesic path as another quantifier for the flatness of a manifold [22]. An estimate of the tangent subspace at a particular data point x_i on the sampled manifold can be obtained using its k-nearest neighborhood $N(x_i)$ by forming the $P \times k$ matrix

$$\mathbf{X}_i = \begin{bmatrix} x_1^i & x_2^i & \dots & x_k^i \end{bmatrix} \tag{15}$$

where $x_j^i \in N(x_i)$. The mean centering of each of the matrices is performed as

$$\hat{\mathbf{X}}_i = \mathbf{X}_i - \frac{1}{k}\mathbf{X}_i\mathbf{1}. \tag{16}$$

The neighborhood covariance matrix for each x_i is then given by

$$\mathbf{W_i} = \hat{\mathbf{X}}_i^T\hat{\mathbf{X}}_i. \tag{17}$$

A local PCA using the covariance matrix gives rise to

$$\mathbf{W_i} = Q\Lambda Q^T \tag{18}$$

where Λ has all the eigenvalues of $\mathbf{W_i}$ in its diagonal. If the intrinsic dimensionality of the manifold is known to be p, then it is known through [22] that the eigenvectors from Q corresponding to the p largest eigenvalues span the tangent space $\mathcal{T}_i$ of the manifold at x_i. All the tangent spaces of a connected manifold have the same intrinsic dimension, which is equal to the intrinsic dimension of the manifold p. In case of a flat manifold, the tangent spaces at all locations are perfectly aligned with each other. The principal or canonical angle [23] between subspaces is used to quantify the alignment. To find the angle between two tangent spaces $\mathcal{T}_i$ and $\mathcal{T}_j$, the inner product matrix $Z = \mathcal{T}_i^T\mathcal{T}_j$ is taken, and a singular value decomposition is performed on Z

$$\mathbf{Z} = U\Sigma V^T \tag{19}$$

to obtain the singular values $\Sigma = \text{diag}(\sigma_1, \sigma_2, \dots)$. The principal angle between tangent subspaces $\mathcal{T}_i$ and $\mathcal{T}_j$ is given by

$$\theta_{i,j} = \min(\cos^{-1}(\sigma_1),\ \cos^{-1}(\sigma_2), \dots). \tag{20}$$

From a differential geometry perspective [24], let $\mathbf{r}(s)$ be an arc length parameterized curve on the manifold M, as shown in Fig. 4. The tangent unit vector is denoted by $\mathbf{r}'(s)$. The second derivative information contained in $\mathbf{r}''(s)$ is obtained by

$$\mathbf{r}''(s) = \lim_{\Delta s \to 0} \frac{\mathbf{r}'(s+\Delta s) - \mathbf{r}'(s)}{\Delta s}. \tag{21}$$

As shown in Fig. 4, $\mathbf{r}'(s)$, $\mathbf{r}'(s+\Delta s)$, and $\mathbf{r}'(s+\Delta s) - \mathbf{r}'(s)$ form an isosceles triangle with the vertex angle $\Delta\psi$. Since $\mathbf{r}'(s)$ is a unit vector and assuming Δs to be very small

$$|\mathbf{r}'(s+\Delta s) - \mathbf{r}'(s)| = \Delta\psi. \tag{22}$$

The absolute value of the second derivative in (21) becomes

$$|\mathbf{r}''(s)| = \lim_{\Delta s \to 0} \frac{\Delta\psi}{\Delta s} = \kappa \tag{23}$$

where κ is popularly called as the curvature. It is an indication of the rate of change of tangent spaces along a geodesic curve on the manifold.

To analyze the trend of the variation of principal angles between tangent spaces, a geodesic curve (shortest path) on the manifold originating from source i_1 to destination i_n and passing through n data points is found out. The principal angles are computed between $\mathcal{T}_1$ and $\mathcal{T}_i$, where $i \in 2, 3 \dots n$ and stored as $\theta_{1,i}$. Similarly, $g_{1,i}$ denotes the estimate of the geodesic distance between x_1 and x_i. From (23), the variation of $\theta_{1,i}$ with respect to $g_{1,i}$ measures the curviness or the rate of change of the tangent space as the manifold is traversed along the geodesic curve. Thus, the metric used is the absolute value of the slope, which is estimated, in discrete sense, as

$$\Phi = \frac{\partial\theta}{\partial g} \approx E\left[\frac{\theta_{1,i} - \theta_{1,i-1}}{g_{1,i} - g_{1,i-1}}\right]. \tag{24}$$

Ideally for a flat manifold, Φ equals to 0, because all the tangent spaces are perfectly aligned with each other. The larger the value, the more curved the manifold is.

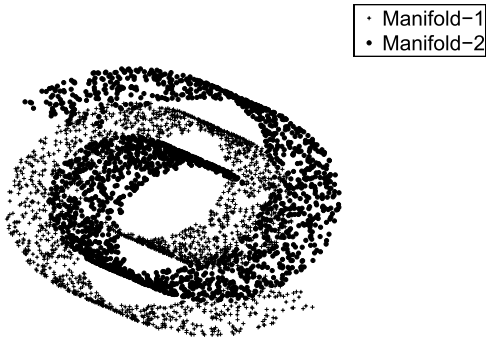

Fig. 5. Two swiss rolls entangled within each other.

TABLE I
DEGREES OF ENTANGLEMENT d AND c MEASURED ON THE TWO MANIFOLDS PROJECTED AT DIFFERENT LAYERS OF A 3-30-30 DBN

Layers	Manifold-1		Manifold-2	
	d	c	d	c
L0 (3)	0.6174	0.7853	0.6390	0.7947
L1 (30)	0.3971	0.4099	0.4294	0.5084
L2 (30)	0.3250	0.2661	0.3622	0.3399

TABLE II
CLASSIFICATION ACCURACY USING FEATURES FROM DIFFERENT LAYERS

Layers (Dimensions)	LDA	QDA
L0 (3)	60.8	60.2
L1 (30)	73.8	98.9
L2 (30)	76.7	97.2
L0+L1 (33)	76.9	99.6
L0+L1+L2 (63)	98.8	100.0

After having come up with measures to quantify the unfolding of individual manifolds, it is worth noting here that the class separability between them is also important to guarantee disentanglement in a classification paradigm. The conventional classification accuracy or any kind of margin-based quantifiers can be used to measure this aspect of disentanglement. The normalized margin [25] for an example x_n is given by

$$m_n = \frac{\|x_n - \mathscr{M}(x_n)\| - \|x_n - \mathscr{H}(x_n)\|}{\|x - \mathscr{M}(x_n)\|} \tag{25}$$

where $\mathscr{M}(x_n)$ is the nearest miss (nearest neighbor from a different class) and $\mathscr{H}(x_n)$ is the nearest hit (nearest neighbor from the same class) of x_n. Maximization of the margin means more separability of individual class clusters. Now, we apply the measures discussed above on a DBN acting on synthetic and real-world image data sets.

V. EXPERIMENTS

A. Experiments With Synthetic Data

Two swiss-roll-type manifolds are entangled with each other, as shown in Fig. 5, to form the data set. It is obvious that no linear hyperplane can separate these two classes in the original 3-D space. As discussed above, if representational features can be found out depicting the underlying dynamics that has led to the construction of this data set, then it may be easier to classify the two. The structure of the underlying low-dimensional manifold is known [21] to be flat or linear for the swiss rolls, since they are intrinsically curvature-less functions which can easily be represented in a flat Euclidean $\mathbb{R}^2$ subspace. In total, $N = 4000$ points are sampled from the two swiss rolls, and the two entanglement quantifying measures d and c are now applied on the output features of each of the three layers in a 3-30-30 DBN formed by stacking two greedily trained continuous RBMs. By experimenting with different choices for a width of the hidden layers, it was seen that the best results were obtained by increasing the number of neurons in the higher layers beyond 30. This might be because of the low dimensionality of the given swiss-roll data. Since the actual manifold structure is known, the shortest path distances using a 25-nearest neighbor graph give a good estimate of the actual geodesic distances. For sensitivity and robustness considerations as discussed in Section IV, the values of α and $\mathscr{S}$ are taken to be 10 and 20, respectively. The input layer is denoted by L0, and the subsequent layers are named L1 and L2. As shown in Table I, both d and c decrease monotonically as we climb up the layers giving an indication that deeper layers tend to unfold the structure of the individual class manifolds.

Remark 1: Higher layers in a deep neural network flatten the individual class manifolds.

As was mentioned earlier, disentanglement need not refer to just flattening or linearization. Thus, the separability of the class manifolds was also studied using the features generated at different layers. It was shown in Table II that when the features of all three layers are concatenated and subject to even a simple linear discriminant analysis, which is a linear classifier, 98.8% classification accuracy could be obtained. Higher layers generate features, which have more separation between the classes and a quadratic classifier, such as quadratic discriminant analysis, can produce perfect classification with all features combined. The features using the stacked continuous RBMs were extracted in a fully unsupervised manner. This also gives us an insight into how these learning networks are helping in proper disentanglement of the contained manifolds in the data.

Remark 2: With a deep learning network, the individual class manifolds cannot only be unfolded, but also their classifiability can be enhanced using the features extracted from higher layers.

Another experiment was conducted to increase the dimensionality P of the swiss-roll data by adding redundant features to it. Raw real-world data, usually noisy and high dimensional ($P \gg N$), often come with features, which are absolutely irrelevant to the learning task. We wanted to check whether the deep learner can perform disentanglement as well when the data contains lots of irrelevant dimensions. Let the original swiss-roll data be $\mathbf{X}$ that belongs to $\mathbb{R}^{N\times 3}$. Redundant dimensions are added in the form of an initially all-zero matrix $\mathbf{Z}$

TABLE III

DEGREES OF ENTANGLEMENT d AND c MEASURED AT DIFFERENT LAYERS OF A 100-1000-1000 DBN APPLIED ONTO THE DIMENSIONS-EXTENDED VERSIONS OF THE MANIFOLDS IN FIG. 5

Layers	d	c
L0 (100)	0.5966	0.7657
L1 (1000)	0.5971	0.7688
L2 (1000)	0.5961	0.7772

Layers	d	c
L0 (100)	0.6225	0.7854
L1 (1000)	0.6236	0.7891
L2 (1000)	0.5936	0.6708

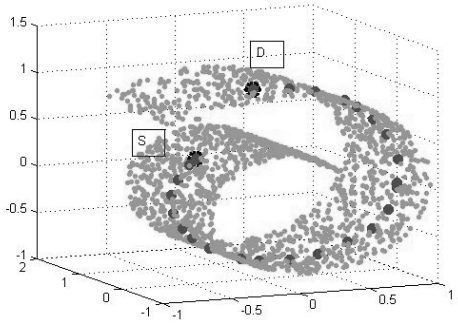

Fig. 6. Geodesic path (in darker dots) between S and D.

of size $\mathbb{R}^{N\times(D-3)}$ to form

$$\mathbf{X}_R = [\mathbf{X} \quad \mathbf{Z}] \tag{26}$$

and thus, $\mathbf{X}_R \in \mathbb{R}^{N\times D}$. An orthonormal matrix $\mathbf{L} \in \mathbb{R}^{D\times D}$ is multiplied with $\mathbf{X}_R$ and summed up with additive noise $\mathcal{N} \in \mathbb{R}^{N\times D}$ to get the rotated manifold projected in a higher dimensional space

$$\mathbf{Y} = \mathbf{X}_R\mathbf{L} + \mathcal{N}. \tag{27}$$

For our experiments, N is kept the same 4000 as before, and D was taken to be 100. In addition, the noise $\mathcal{N}$ was considered to be zero mean Gaussian with a small variance, that is, $\sim$1% of that of the original data $\mathbf{X}$. This newly generated data set $\mathbf{Y}$ that belongs to $\mathbb{R}^{4000\times100}$ is now fed to a continuous RBM-based neural network of size 100-1000-1000. As can be seen with the entanglement measures listed in Table III, no significant flattening is obtained, since the values of d and c do not vary along the layers for both the class manifolds. This experiment was also done in the absence of any added noise, and the trend of the measures across the layers was again similar. It means that too many nuisance dimensions in the data confuse the deep learning model.

Remark 3: Disentanglement is severely degraded in the presence of a large number of redundant dimensions in input data.

Subsequently, the curvature-based metric Φ was calculated using the features at different layers. Since the swiss roll is known to be a two-manifold, the intrinsic dimensionality p was taken to be 2. To estimate the tangent spaces, the value of k in (15) was taken to be 5. For each of the two manifolds, source (S) and destination (D) data examples were chosen that were geodesically distant enough so that a curve connecting them can traverse most of the manifold, as shown in Fig. 6. Alignment of the tangent spaces along the geodesic path with respect to the tangent space at source was analyzed, and the metric Φ was calculated as per (24) and reported in Table IV. Since the DBN creates a one-to-one representational mapping, the same data nodes were also used as S and D while computing the shortest path and the curvature Φ at different layers of the autoencoder. A clear decrease in Φ as we go up the layers reaffirms Remark 1 stating manifold unfolding in deeper layers.

TABLE IV

CURVATURE-BASED DEGREE OF ENTANGLEMENT Φ AT DIFFERENT LAYERS OF 3-30-30 DBN

Layers	Φ for Manifold-1
L0 (3)	87.3768
L1 (30)	65.4784
L2 (30)	42.7480

Layers	Φ for Manifold-2
L0 (3)	88.3762
L1 (30)	77.1275
L2 (30)	39.7518

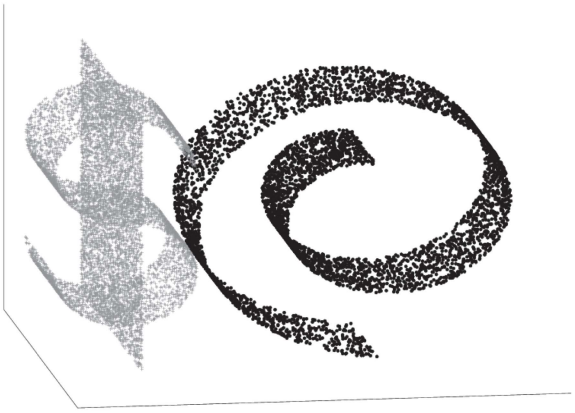

Fig. 7. Data set of two classes where the one in the shape of a dollar (\$) contains a mixture of manifolds in itself.

TABLE V

DEGREES OF ENTANGLEMENT d AND c MEASURED ON THE TWO CLASSES IN FIG. 7 AT DIFFERENT LAYERS OF A 3-30-30 DBN

LAYERS	Swiss-roll Manifold		\$-shaped Manifold	
	d	c	d	c
L0 (3)	0.5356	0.6708	0.2148	0.1548
L1 (30)	0.4975	0.6178	0.2196	0.1550
L2 (30)	0.3358	0.3110	0.2114	0.1272

It is important to note here that the measures of entanglement discussed above have severe limitations and may specially fail to denote unfolding when each class, in itself, consists of a mixture of manifolds or self-intersecting ones. A dollar-shaped (\$) manifold, which can be considered to be either self-intersecting or a combination of an S-shaped and a linear (vertically aligned) manifold, belongs to one of the classes, and the other class is represented by a swiss roll in Fig. 7. If the unfolding measures c and d are measured across the layers of a stacked RBM-based 3-30-30 network for the dollar-shaped manifold, then the variations in the structure of the manifold cannot be observed in Table V. However, a single-connected component, such as the swiss roll, does exhibit unfolding and reduction of entanglement measures as has been shown previously too.

Therefore, it is important to enlist the explicit set of assumptions that are made on the data while applying these measures of entanglement. These are as follows.

1) In its original space, the data belonging to each class lie on a single-connected manifold. The measures will fail to quantify disentanglement if each class, in itself, is a mixture of multiple disconnected manifolds.
2) Each of the class manifolds is considered to be smoothly varying and without self-intersections.
3) A completely unfolded manifold is considered as a linear or Euclidean subspace in the projected space.
4) The training data represent a densely sampled version of the original manifold such that all the relevant variations are captured by choosing the neighborhood size to form a nearest neighbor graph.

B. Experiments With Face Images

The Olivetti face data set is a popularly used database of human faces that contains ten gray-scale images each of 40 different people, making it 400 images in total. We augmented this data set following the lines of [7] by applying rotations (-25° to $+25^\circ$), translation, and resampling. The final cropped input to the DBN contains 20 400 images of 25×25 pixels each. In the experiments, each face is treated as a separate manifold, and the pixel intensity values represent a feature vector for each image. All the images were mean centered and normalized to make average standard deviation to be 1. A three-layered DBN 625-2000-625 was designed by stacking two RBMs on top of one another and greedily training them to form an autoencoder. Another output softmax layer containing 40 nodes may also be added in order to perform the task of classification. However, the current experiment aims at analyzing the change in the structure of the data using the hidden layers. The first RBM is a Gaussian-binary RBM, since the gray-scale images of faces can be better modeled as Gaussian real values rather than binary, while the latent or hidden variables were taken to be binary units. The energy function of such an RBM turns out to be

$$E(x,h) = \sum_{\text{vis}} \frac{(x_i - a_i)^2}{2\sigma^2} - c'h - \sum_{i,j} W_{ij} \frac{x_i h_j}{\sigma_i \sigma_j}. \quad (28)$$

In addition, the output code layer was modeled as linear units. If the deep learner can actually disentangle the individual face manifolds, then a reduction of the flattening metrics c and d and an increase in separability margin will be observed in the projected code layer as compared with the input layer. For fairness of comparison, the dimensionality of input and code layers were kept same, though the measures are independent of the dimension of the data space. Of the 40 subjects, four faces manifolds were chosen at random, and the values of c and d measured at the input and the projected code layer were enlisted in Table VI. A decrease in the measures signifies the occurrence of flattening caused due to unsupervised deep training with respect to Remark 1. On an average over all the faces, c and d recorded a decrease of 18.92% and 33.54%, respectively, as compared with their values on the raw input.

TABLE VI

COMPARING d AND c FOR SOME OF THE FACE MANIFOLDS BETWEEN THE INPUT AND PROJECTED CODE LAYERS OF A 625-2000-625 DBN

Face Manifolds	c		d	
	Input	Projected	Input	Projected
	0.1954	0.1670	0.9091	0.6722
	0.1305	0.0951	1.0452	0.6606
	0.1630	0.1355	0.9943	0.6581
	0.2242	0.2103	1.0304	0.6990

TABLE VII

COMPARISON OF MARGIN VALUES USING FEATURES FROM DIFFERENT LAYERS OF THE DBN

Layers	Margin
L0 (625)	0.7019
L1 (2000)	0.8084
L2 (625)	0.8579

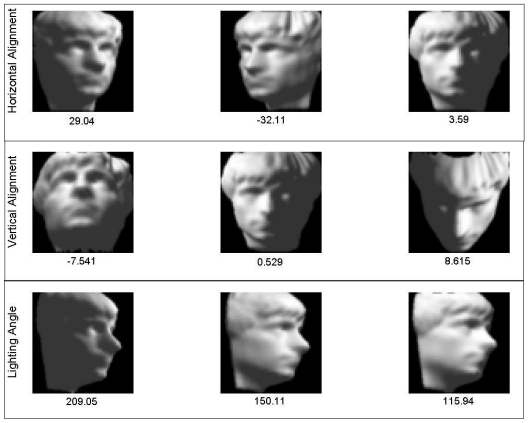

Fig. 8. Images from the ISOMAP face data set with respect to the pose variables in the first two rows and lighting angle in the last row.

Next, the average normalized margin was observed across the layers in Table VII, and an increase in the values is indicative of the increasing separability of class manifolds with depth.

Though it is hypothesized that a deep model can extract the governing (hidden) factors of variation in the data, the lack of ground truth for most real-world data hinders its provability. Hence, we considered experimenting on an image data set, with known ground-truth factors of variation, for which manifold learning methods have been previously implemented successfully to do dimensionality reduction. The ISOMAP face data set [21] consists of 698 images of a fixed face rendered under different pose (horizontal and vertical alignment) and lighting (azimuthal angle of the lighting source) condi-

TABLE VIII

CROSS CORRELATION OF 3-D EMBEDDINGS OBTAINED USING CLASSICAL PCA, ISOMAP, AND DBN+PCA WITH GROUND TRUTH FOR HORIZONTAL POSE, VERTICAL POSE, AND LIGHTING DIRECTION

Hidden Factors	PCA	ISOMAP	DBN+PCA
Horizontal Pose	0.75	0.98	0.9143
Vertical Pose	0.33	0.901	0.673
Lighting Angle	0.68	0.927	0.8629

tions. Although each image (64 × 64 pixels) shown in Fig. 8 lies on a 4096-D input space, the intrinsic dimensionality of the manifold defining all the images is rather just three, given by the two pose and one lighting angle variables. Given the complexity of the manifold embedded in such a high-dimensional space, it is intuitive to note that a linear dimensionality reduction method, such as PCA, would fail to recover the values of the causing factors. ISOMAP, on the other hand, is a nonlinear manifold learning algorithm, which first forms a nearest neighbor graph, computes shortest path distances between each pair of images, and finally uses these distances to perform an isometric low-dimensional embedding using eigendecomposition. In Table VIII, 3-D embeddings of the face image data set were obtained using both PCA and ISOMAP, and the best match cross correlation with the ground-truth values of the two pose and lighting angle variables were reported. As expected, the PCA resulted in confused embeddings showing very low correlation with the true parameters, while very high correlation was observed with the embeddings obtained through ISOMAP.

The reason behind the failure of PCA is nonlinearity of the data in its original dimensional space. Had the data been on a linear or flat manifold (such as a plane in $\mathbb{R}^3$), dimensionality reduction could have easily been obtained through the linear methods. The unfolding of manifolds using deep architectures has been shown so far on both synthetic swiss-roll type as well as real-world face data sets. This property of deep learning can well be leveraged to flatten the ISOMAP face manifold first and then apply linearity assumption-based PCA to recover the hidden parameters controlling the data generation. All images were downsampled by two and fed to a 1024-2000-1000-300-50 autoencoder formed by stacking RBMs on top of one another just like in the previous case. A 3-D PCA reduction is applied onto the final code layer output, and the prominent eigenvectors are compared with the ground-truth pose and lighting values for each image. Again, cross correlation with the factors of variation is taken as a metric to evaluate the model's performance.

The deep unsupervised learning plus linear dimensionality reduction method is undoubtedly better than just PCA but still lags behind the performance of ISOMAP. The possible reason is that the objective function of ISOMAP is explicitly designed to cater to manifold embedding needs. However, the results with a stacked RBM architecture can rather be considered as a by-product of the learning algorithm. Involving manifold prior-based regularization in the optimization function of the autoencoder may improve the deep learner's performance significantly.

TABLE IX

c FOR DIGIT MANIFOLDS AT DIFFERENT LAYERS AFTER UNSUPERVISED PRETRAINING

DIGIT	**L0(784)**	**L1(1000)**	**L2(1000)**	**L3(1000)**
0	0.2625	0.2230	0.2428	0.2084
2	0.4123	0.3707	0.3734	0.3518
4	0.4126	0.3564	0.3830	0.3293
7	0.2994	0.2542	0.2712	0.2445
9	0.3209	0.2496	0.2864	0.2493

TABLE X

d FOR DIGIT MANIFOLDS AT DIFFERENT LAYERS AFTER UNSUPERVISED PRETRAINING

DIGIT	**L0(784)**	**L1(1000)**	**L2(1000)**	**L3(1000)**
0	2.1063	2.0355	2.0158	1.9992
2	2.3745	2.3960	2.3418	2.3672
4	2.3732	2.3359	2.3208	2.2805
7	2.1508	2.0696	2.0669	2.0072
9	2.2755	2.1841	2.1980	2.1345

Fig. 9. Digit 7 (a) without a middle stick and (b) with a middle stick.

Remark 4: With a deep generative network, the hidden factors governing the variations in the data can be recovered, which are also representative of the true intrinsic structure of the manifold.

C. Experiments With Images of MNIST Handwritten Digits

The MNIST database of handwritten digits [26] has a training set of 60 000 images and a test set of 10 000 images of the ten numeric digits written by various people. Each digit has been normalized and centered in a 28 × 28 image. The thickness, height, angular alignment, and relative position in a frame are some of the intrinsic hidden properties that govern the generation of the examples for each digit manifold. The entire data set of images is considered as a collection of blended manifolds plus additive noise. A multilayer 784-1000-1000-1000 DBN was set up and pretrained layer by layer as binary–binary RBMs without any label supervision. The disentanglement measures c and d, as reported in Tables IX and X for five digits using a six nearest neighbor graph, show a decreasing trend, though not monotonic, as the deeper layers are traversed. The parameters for robustness (α) and sensitivity ($\mathscr{S}$) were also taken to be 10 and 20, respectively. Φ was not calculated on this data set, since it requires the knowledge of the true intrinsic dimensionality. However,

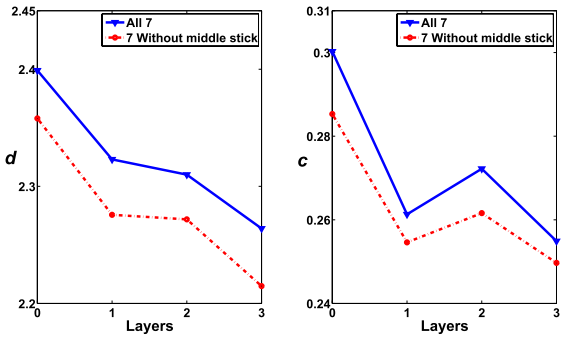

Fig. 10. d and c for whole class and a subclass of digit 7.

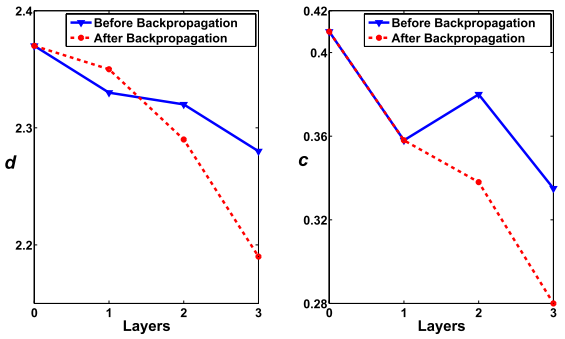

Fig. 11. d and c across the layers for the manifold of digit 4 before and after supervised backpropagation.

TABLE XI

c FOR DIGIT MANIFOLDS AT DIFFERENT LAYERS AFTER SUPERVISED FINE-TUNING USING BACKPROPAGATION

DIGIT	L0(784)	L1(1000)	L2(1000)	L3(1000)
0	0.2625	0.2042	0.1791	0.1612
2	0.4123	0.3535	0.3144	0.2747
4	0.4126	0.3576	0.3333	0.2912
7	0.2994	0.2551	0.2361	0.2069
9	0.3209	0.2788	0.2551	0.2266

TABLE XII

d FOR DIGIT MANIFOLDS AT DIFFERENT LAYERS AFTER SUPERVISED FINE-TUNING USING BACKPROPAGATION

DIGIT	L0(784)	L1(1000)	L2(1000)	L3(1000)
0	2.1063	2.0577	2.0243	1.9629
2	2.3745	2.4215	2.3604	2.3165
4	2.3732	2.3482	2.2997	2.1851
7	2.1508	2.0912	2.0846	1.9878
9	2.2755	2.2395	2.2199	2.1121

experiments can also be conducted using a guess value of the parameter.

If each class consists of multiple disconnected manifolds, then the distances considered between some pairs of images, which do not belong to the same manifold, may lead to discrepancies in the estimates of the measures as it violates the assumptions mentioned earlier. Unlike the swiss-roll example in Section V-A, describing all images belonging to a unique digit as a single manifold may be debatable. Thus, we tried to find subclasses among the digits characterized with known physical appearance features and then evaluate c and d over them. For example in Fig. 9, the digit 7 can be broadly written in two different styles—either without a middle stick or with it. When only those examples of the digit 7 falling under category Fig. 9(a) were considered, both c and d were found to be lower than those for the combined class and also experienced the same trend that deeper layers have more unfolding, as shown in Fig. 10.

It is also shown in Tables XI and XII that after supervised backpropagation (using another softmax output layer of ten nodes for each of the ten digits), the model not only retains the disentanglement, but also improves upon it while increasing the discriminative abilities between the class manifolds too.

TABLE XIII

COMPARISON OF MARGIN VALUES USING FEATURES FROM DIFFERENT LAYERS OF A 784-1000-1000-1000 DEEP NETWORK

Layers (Dimensions)	After Pre-training	After backpropagation
L0 (784)	0.2754	0.2754
L1 (1000)	0.3189	0.3303
L2 (1000)	0.3201	0.3498
L3 (1000)	0.3503	0.4158

Though the latter is quite expected for a discriminative procedure like supervised backpropagation, the observation that the unfolding of manifolds also improves with it is rather surprising and interesting. The final test classification error was 1.12% that matches with the results in [7]. In addition, it was shown in [10] that concatenation of raw input with higher representations was more linearly discriminative. Thus, it also explains that the deep network produces a set of unfolded manifolds, which are also more separable than the original input manifolds. A basic problem with the conventional multilayer neural networks was that the lower layers remained undertrained due to the problem of vanishing gradient. Thus, the main contribution of the generative pretraining using RBMs can be thought of better training of the lower layers for which we see a clear drop in the entanglement measures (lower in L1 as compared with L0). It is intuitive that the unsupervised stage of a DBN, which is based on the sampling-based distribution learning technique, loses a lot of relevant information while moving up the layers. Thus, we see a zigzag structure in the plots of Fig. 11 instead of an ideal monotonic decrease. A supervised and discriminative backpropagation pronounces the disentanglement process for the higher layers for which we see a more expected monotonic decrease of entanglement measures as we go up the layers.

Remark 5: Unsupervised pretraining (generative) helps in disentangling the class manifolds in the lower layers of a deep learner, while the upper layers are better disentangled when it is subject to a supervised backpropagation (discriminative). A combination of the two helps boosts the overall performance.

Now that the evidence for the unfolding of individual class manifolds is established, we look at the separability aspect of disentanglement by comparing the expected value of the margin estimator taken over all observations. It was seen pre-

viously that the deep layers tend to generate hidden features of importance in all layers, and these features provide the intrinsic identity to each class making them more separable. As shown clearly in Table XIII, there is a rise in the margin values when the deeper layers are considered as the feature space; thus indicating what was pointed out in Remark 2. In [10], classification accuracy using a linear support vector machine classifier was shown to be competitive enough while using all layerwise features combined. It is interesting to see here that the maximum impact by the discriminative backpropagation is caused in the higher layers like L3 (which is penultimate to the target layer of ten label nodes). This suggests that a combination of generative modules at the first followed by discriminative modules can actually perform better in the task of classification or clustering. This is also the reason why an unsupervised pretraining helped gain higher classification accuracy as compared with a traditional multilayer neural network that lacked a pretrained generative module.

Remark 6: The unfolding of class manifolds through deep architectures also creates an expansion of the feature space in which the classes are more separable from each other.

VI. Conclusion

The extraction of the governing factors of variation using deep neural networks has been discussed in the literature before. In this paper, manifold-based measures were proposed and tested to justify the hypothesis of unfolding and subsequent separation of intrinsically low-dimensional manifolds in the data. Experiments on synthetic and real-world data sets revealed the gradual disentanglement of individual class manifolds at deeper layers following the unsupervised pretraining and that got even better when the network was subject to a discriminative backpropagation-based fine-tuning. This suggests that the fundamental function of the first-generate-then-discriminate models is to first-unfold-then-separate each individual manifold present in the data. This insight explains why an unsupervised pretraining has helped overcome the deficiencies of the traditional neural networks. The change in the entanglement values in case of real-world image data sets was rather miniscule. It may be due to Remark 3, which suggests that the presence of too many redundant features in each layer may hinder the learning process. Moreover, the remarks discussed in this paper also explain the performance gain achieved by the other deep learning methods, even those which are not entirely based on a neural network framework. For example, in [17], a sparse random projection-based dimension reducer is first employed before feeding the projected data into a supervised neural network. It has been researched before that by virtue of the Johnson–Lindenstrauss lemma [27], under certain conditions, random projections can lead to low-dimensional embedding of points such that the distances between points are nearly preserved. This can also lead to manifold disentanglement which can subsequently aid any discriminative learner, such as the neural networks. One immediate application of this paper can be better interpolation between examples, such as face warping, using features from higher layers. Enforcing disentanglement as a regularization constraint in the optimization objective can also lead to even superior performance. Algorithms, such as the contractive autoencoder [28] and semisupervised deep learning [29], have indeed applied a manifold-based penalty in their objective functions and have led to better results with real-world data sets. It was also shown in this paper that the unfolding of manifolds is limited to the lower layers of an unsupervised deep network, while the separability is prominent mostly in the higher layers during supervised training. This fact can be used to isolate both the generative and discriminative processes by limiting them only to the lower and higher layers, respectively, which may ultimately lead to faster learning.

References

[1] X. Glorot and Y. Bengio, "Understanding the difficulty of training deep feedforward neural networks," in *Proc. 19th Int. Conf. Artif. Intell. Statist.*, Sardinia, Italy, 2010, pp. 249–256.

[2] Y. N. Dauphin, R. Pascanu, C. Gulcehre, K. Cho, S. Ganguli, and Y. Bengio, "Identifying and attacking the saddle point problem in high-dimensional non-convex optimization," in *Proc. Adv. Neural Inf. Process. Syst.*, Montreal, QC, Canada, 2014, pp. 2933–2941.

[3] B. Schölkopf and A. J. Smola, *Learning With Kernels: Support Vector Machines, Regularization, Optimization, and Beyond*. Cambridge, MA, USA: MIT Press, 2002.

[4] L. Deng and D. Yu, "Deep learning: Methods and applications," *Found. Trends Signal Process.*, vol. 7, nos. 3–4, pp. 197–387, Jun. 2014.

[5] T. Joachims, "Text categorization with support vector machines: Learning with many relevant features," in *Proc. 10th Eur. Conf. Mach. Learn.*, Chemnitz, Germany, 1998, pp. 137–142.

[6] Y. Bengio, O. Delalleau, and N. L. Roux, "The curse of highly variable functions for local kernel machines," in *Proc. Adv. Neural Inf. Process. Syst.*, Vancouver, BC, Canada, 2005, pp. 107–114.

[7] G. E. Hinton and R. R. Salakhutdinov, "Reducing the dimensionality of data with neural networks," *Science*, vol. 313, no. 5786, pp. 504–507, 2006.

[8] L. Wan, M. Zeiler, S. Zhang, Y. LeCun, and R. Fergus, "Regularization of neural networks using DropConnect," in *Proc. 30th Int. Conf. Mach. Learn.*, Atlanta, GA, USA, Jun. 2013, pp. 1058–1066.

[9] G. Hinton *et al.*, "Deep neural networks for acoustic modeling in speech recognition: The shared views of four research groups," *IEEE Signal Process. Mag.*, vol. 29, no. 6, pp. 82–97, Nov. 2012.

[10] Y. Bengio, G. Mesnil, Y. Dauphin, and S. Rifai, "Better mixing via deep representations," in *Proc. 30th Int. Conf. Mach. Learn.*, Atlanta, GA, USA, Jun. 2013, pp. 552–560.

[11] Y. Bengio, A. Courville, and P. Vincent, "Representation learning: A review and new perspectives," *IEEE Trans. Pattern Anal. Mach. Intell.*, vol. 35, no. 8, pp. 1798–1828, Aug. 2013.

[12] Y. She. (Mar. 2014). "Selectable factor extraction in high dimensions." [Online]. Available: http://arxiv.org/abs/1403.6212

[13] Q. Huang and D. O. Wu, "Flatten a curved space by kernel [applications corner]," *IEEE Signal Process. Mag.*, vol. 30, no. 5, pp. 132–142, Sep. 2013.

[14] I. J. Goodfellow, Q. V. Le, A. M. Saxe, H. Lee, and A. Y. Ng, "Measuring invariances in deep networks," in *Proc. Adv. Neural Inf. Process. Syst.*, vol. 22. 2009, pp. 646–654.

[15] M. A. Carreira-Perpinan and G. E. Hinton, "On contrastive divergence learning," in *Proc. 10th Int. Workshop Artif. Intell. Statist.*, Bridgetown, Barbados, 2005, pp. 33–40.

[16] H. Chen and A. F. Murray, "Continuous restricted Boltzmann machine with an implementable training algorithm," *IEE Proc.-Vis., Image Signal Process.*, vol. 150, no. 3, pp. 153–158, Jun. 2003.

[17] G. E. Dahl, J. W. Stokes, L. Deng, and D. Yu, "Large-scale malware classification using random projections and neural networks," in *Proc. IEEE Int. Conf. Acoust., Speech Signal Process.*, Vancouver, BC, Canada, May 2013, pp. 3422–3426.

[18] J. M. Lee, *Introduction to Smooth Manifolds*. New York, NY, USA: Springer-Verlag, 2002.

[19] L. Cayton, "Algorithms for manifold learning," Univ. California, San Diego, San Diego, CA, USA, Tech. Rep. CS2008-0923, 2005.

[20] R. Basri and D. W. Jacobs, "Lambertian reflectance and linear subspaces," *IEEE Trans. Pattern Anal. Mach. Intell.*, vol. 25, no. 2, pp. 218–233, Feb. 2003.
[21] J. B. Tenenbaum, V. de Silva, and J. C. Langford, "A global geometric framework for nonlinear dimensionality reduction," *Science*, vol. 290, no. 5500, pp. 2319–2323, 2000.
[22] Z. Zhang and H. Zha, "Principal manifolds and nonlinear dimensionality reduction via tangent space alignment," *SIAM J. Sci. Comput.*, vol. 26, no. 1, pp. 313–338, 2005.
[23] A. V. Knyazev and M. E. Argentati, "Principal angles between subspaces in an *A*-based scalar product: Algorithms and perturbation estimates," *SIAM J. Sci. Comput.*, vol. 23, no. 6, pp. 2008–2040, 2002.
[24] E. Kreyszig, *Differential Geometry*. New York, NY, USA: Dover, 1991.
[25] Y. Sun and D. Wu, "Feature extraction through local learning," *Statist. Anal. Data Mining*, vol. 2, no. 1, pp. 34–47, Jul. 2009.
[26] Y. LeCun, L. Bottou, Y. Bengio, and P. Haffner, "Gradient-based learning applied to document recognition," *Proc. IEEE*, vol. 86, no. 11, pp. 2278–2324, Nov. 1998.
[27] D. Achlioptas, "Database-friendly random projections: Johnson–Lindenstrauss with binary coins," *J. Comput. Syst. Sci.*, vol. 66, no. 4, pp. 671–687, Jun. 2003.
[28] S. Rifai, P. Vincent, X. Muller, X. Glorot, and Y. Bengio, "Contractive auto-encoders: Explicit invariance during feature extraction," in *Proc. 28th Int. Conf. Mach. Learn.*, Bellevue, WA, USA, 2011, pp. 833–840.
[29] J. Weston, F. Ratle, and R. Collobert, "Deep learning via semi-supervised embedding," in *Proc. 25th Int. Conf. Mach. Learn.*, Helsinki, Finland, 2008, pp. 1168–1175.

Pratik Prabhanjan Brahma received the B.Tech. degree in electronics and electrical communication engineering and the M.Tech. degree in telecommunication systems engineering from IIT Kharagpur, Kharagpur, India, in 2011. He is currently pursuing the Ph.D. degree in electrical and computer engineering with the University of Florida, Gainesville, FL, USA.

His current research interests include machine learning, computer vision, data science, statistics, and network science.

Dapeng Wu (S'98–M'04–SM'06–F'13) received the Ph.D. degree in electrical and computer engineering from Carnegie Mellon University, Pittsburgh, PA, USA, in 2003.

He is currently a Professor with the Department of Electrical and Computer Engineering, University of Florida, Gainesville, FL, USA. His current research interests include networking, communications, signal processing, computer vision, machine learning, smart grid, and information and network security.

Dr. Wu received the University of Florida Research Foundation Professorship Award in 2009, the AFOSR Young Investigator Program (YIP) Award in 2009, the ONR YIP Award in 2008, the NSF CAREER Award in 2007, the IEEE TRANSACTIONS ON CIRCUITS AND SYSTEMS FOR VIDEO TECHNOLOGY Best Paper Award in 2001, and the best paper awards in the IEEE GLOBECOM 2011 and the International Conference on Quality of Service in Heterogeneous Wired/Wireless Networks in 2006. He serves as an Associate Editor of the IEEE TRANSACTIONS ON CIRCUITS AND SYSTEMS FOR VIDEO TECHNOLOGY and the IEEE TRANSACTIONS ON SIGNAL AND INFORMATION PROCESSING OVER NETWORKS.

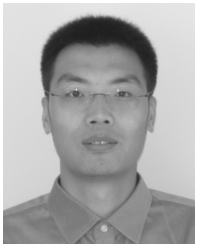

Yiyuan She received the B.S. degree in mathematics and the M.S. degree in computer science from Peking University, Beijing, China, in 2000 and 2003, respectively, and the Ph.D. degree in statistics from Stanford University, Stanford, CA, USA, in 2008.

He is currently an Associate Professor with the Department of Statistics, Florida State University, Tallahassee, FL, USA. His current research interests include high-dimensional statistics, machine learning, multivariate statistics, robust statistics, statistics computing, and network science.